Available online at www.sciencedirect.com

SCIENCE DIRECT®

PERGAMON

International Journal of Multiphase Flow 29 (2003) 395–409

International Journal of Multiphase Flow

www.elsevier.com/locate/ijmulflow

Experimental study of interfacial area transport of bubbly flow in small-diameter tube

T. Takamasa [a,*], T. Goto [a], T. Hibiki [b], M. Ishii [c]

[a] *Faculty of Marine Science, Tokyo University of Mercantile Marine, Etchujima, Koto, Tokyo 135-8533, Japan*
[b] *Research Reactor Institute, Kyoto University, Kumatori, Sennan, Osaka 590-0494, Japan*
[c] *School of Nuclear Engineering, Purdue University, 400 Central Drive, West Lafayette, IN 47907-2017, USA*

Received 21 May 2001; received in revised form 10 December 2002

Abstract

In relation to the development of the interfacial area transport equation, this study was aiming at collecting accurate data sets on axial developments of local flow parameters such as void fraction, interfacial area concentration, and gas velocity. The local flow measurements of air–water bubbly flow in a vertical 9-mm-diameter tube were performed by means of a stereo image-processing method. A total of three data sets were acquired consisting of two gas flow rates, 0.013–0.052 m/s, and two liquid flow rates, 0.58–1.0 m/s at six axial locations. The data would be used for the development of reliable constitutive relations which reflect the true transfer mechanisms in two-phase flow.

Keywords: Interfacial area transport; Interfacial area concentration; Bubbly flow; Two-fluid model

1. Introduction

In 1996, the workshop on transient thermal-hydraulic and neutronic code requirements in the field of the nuclear safety was held to discuss (1) current and prospective plans of thermal hydraulic codes development; (2) current and anticipated uses of thermal-hydraulic codes; (3) advances in modeling of thermal-hydraulic phenomena and associated additional experimental needs; (4) numerical methods in multi-phase flows; and (5) programming language, code architectures and user interfaces (Ebert, 1997). The workshop consensus identified some important

* Corresponding author. Tel.: +81-3-5245-7406; fax: +81-3-5245-7410.
E-mail address: takamasa@ipc.tosho-u.ac.jp (T. Takamasa).

0301-9322/03/$ - see front matter
doi:10.1016/S0301-9322(02)00167-2

action items to be addressed by the international community in order to maintain and improve the calculation capability. One of the important action items was the introduction of the interfacial area transport equation to the interfacial transfer terms in the two-fluid model.

The interfacial area transport equation can be obtained by considering the fluid particle number density transport equation analogous to Boltzmann's transport equation (Kocamustafaogullari and Ishii, 1995). It can replace the traditional flow regime maps and regime transition criteria that do not dynamically represent the changes in interfacial structure. The changes in the two-phase flow structure are predicted mechanistically by introducing the interfacial area transport equation. Thus, a successful development of the interfacial area transport equation can make a quantum improvement in the two-fluid model formulation.

In order to develop the interfacial area transport equation, considerable efforts have recently been made (1) to formulate the interfacial area transport equation, (2) to develop measurement techniques for local flow parameters, (3) to construct data bases of axial developments of local flow parameters, (4) to model sink and source terms in the interfacial area transport equation, and (5) to improve system analysis codes by implementing the interfacial area transport equation. The present status of the development of the interfacial area transport equation was extensively reviewed in the previous paper (Hibiki and Ishii, 2002). It has been demonstrated that the interfacial area transport equation can give a good prediction for bubbly flows in vertical tubes with medium tube diameters (25.4–50.8 mm). However, to generalize the interfacial area transport equation, further analytical and experimental studies should be performed in other flow regimes as well as two-phase flows in various channels such as an elbow, a T-junction, and large and small channels. From this point of view, this study is aiming at collecting accurate data sets on axial developments of local flow parameters such as void fraction, interfacial area concentration, and gas velocity in a relatively small diameter tube with an inner diameter of 9.0 mm.

2. Interfacial area transport equation

Kocamustafaogullari and Ishii (1995) derived the interfacial area transport equation by considering the fluid particle number density transport equation analogous to Boltzmann's transport equation. As a general approach, two-group interfacial area transport equations have recently been proposed by treating the bubbles in two groups such as the spherical/distorted bubble group and the cap/slug bubble group (Wu et al., 1998; Hibiki and Ishii, 2000b). This approach results in two interfacial area transport equations that involve the inner and inter group interactions. However, the two-group transport equations can be reduced to one-group for a bubbly flow where the bubbles can be assumed to be equivalent in diameter. Thus, the one-group interfacial area transport equation is given as:

$$\frac{\partial a_i}{\partial t} + \frac{d}{dz}(a_i v_G) = \frac{1}{3\psi}\left(\frac{\varepsilon}{a_i}\right)^2(\phi_B - \phi_C + \phi_P) + \left(\frac{2a_i}{3\varepsilon}\right)\left\{\frac{\partial \varepsilon}{\partial t} + \frac{d}{dz}(\varepsilon v_G)\right\}$$
$$= \Phi_B + \Phi_C + \Phi_P + \Phi_V, \quad (1)$$

where

$$\Phi_B \equiv \frac{1}{3\psi}\left(\frac{\varepsilon}{a_i}\right)^2 \phi_B, \qquad \Phi_C \equiv \frac{1}{3\psi}\left(\frac{\varepsilon}{a_i}\right)^2 \phi_C, \qquad \Phi_P \equiv \frac{1}{3\psi}\left(\frac{\varepsilon}{a_i}\right)^2 \phi_P, \quad \text{and}$$

$$\Phi_V \equiv \left(\frac{2a_i}{3\varepsilon}\right)\left\{\frac{\partial \varepsilon}{\partial t} + \frac{d}{dz}(\varepsilon v_G)\right\}.$$

The symbols of a_i, t, v_G, z, ψ, and ε denote the interfacial area concentration, the time, the gas velocity, the axial position, a factor depending on the bubble shape ($\psi = 1/(36\pi)$ for spherical bubbles), and the void fraction, respectively. ϕ_B, ϕ_C, and ϕ_P are the rates of change of bubble number density due to bubble breakup, bubble coalescence, and phase change, respectively. Φ_B, Φ_C, Φ_P, and Φ_V are the rates of change of interfacial area concentration due to bubble breakup, bubble coalescence, phase change, and void transport, respectively. Under no phase change condition, ϕ_P and Φ_P become zero.

In the previous study (Hibiki and Ishii, 2000a), the major mechanism of the interfacial area transport of bubbly flow in medium tubes (25.4–50.8 mm) where the bubble size-to-tube diameter ratio, D_b/D, was relatively low ($D_b/D \leqslant 0.12$) have been modeled successfully by the bubble coalescence due to the bubble random collisions driven by liquid turbulence, and the bubble breakup due to the impact of turbulent eddies. On the other hand, in a relatively small diameter tube, the bubble size-to-tube diameter ratio may be relatively high, and it is anticipated that the radial motion of bubbles may be restricted by the presence of the tube wall. Thus, the interfacial area transport mechanism in a relatively small diameter tube may be quite different from that in a medium tube. In what follows, the visual observation and local flow measurements will be performed to confirm the difference in the interfacial area transport mechanism between small and medium tubes.

3. Experiment

Fig. 1 shows a schematic diagram of a two-phase flow loop used in the present experiment. The test section was a round tube made of acrylic resin. Its inner diameter, D, and length, L, were 9 and 945 mm, respectively. Air was supplied by a compressor and was introduced into a mixing chamber through the bubble generator shown in Fig. 2. Tap water was purified with a pure-water generator to electrical conductivity of less than 1 μs/cm. The air and purified water were mixed in the mixing chamber, and the mixture flowed upward through the test section. After flowing through the test section, air was released into the atmosphere through a separator, while the water was circulated by a centrifugal pump. The water temperature was maintained at 20 ± 0.5 °C by a submerged heater and a cooler in a water reservoir. The air and water flow rates were measured with rotameters.

Local measurements of flow parameters such as void fraction, interfacial area concentration and gas velocity were performed by a stereo image-processing method. In the stereo image-processing method, a bubble shape was reconstructed by two simultaneous images taken from two different directions with an assumption of an ellipsoidal bubble shape. The angle between two images was set at 90° in the present experiment. This method was valid at low void fraction ($\langle \varepsilon \rangle \leqslant 10\%$ for a 9-mm diameter tube) and liquid velocity ($\langle j_L \rangle \leqslant 1$ m/s) where the bubble

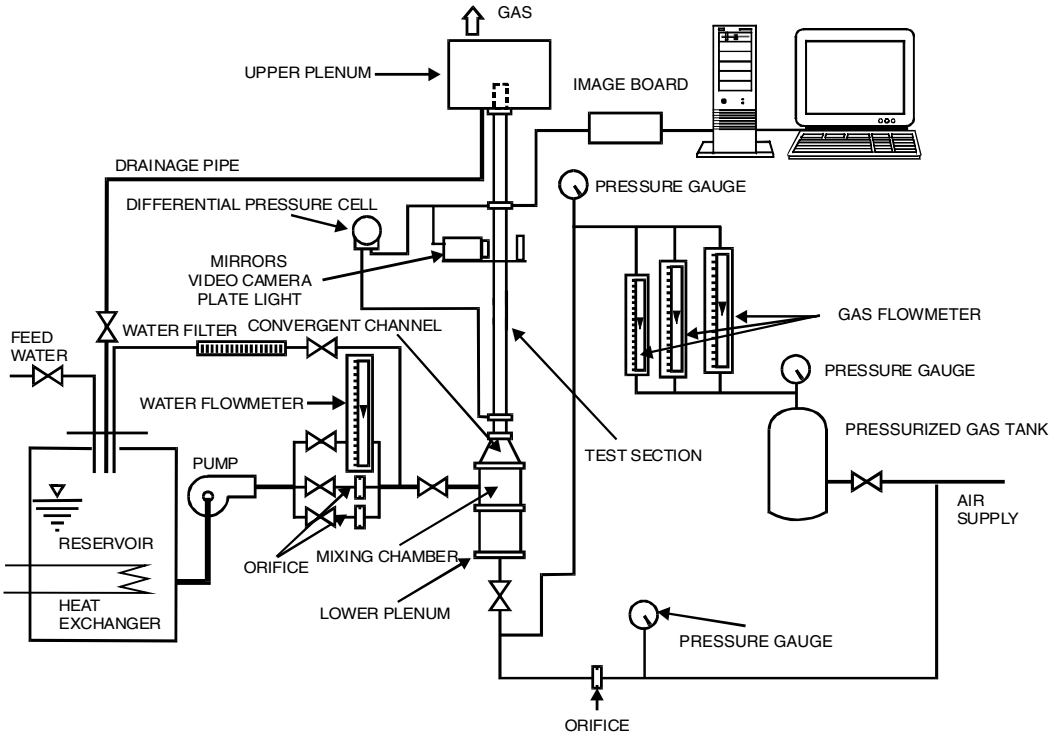

Fig. 1. Schematic diagram of experimental loop.

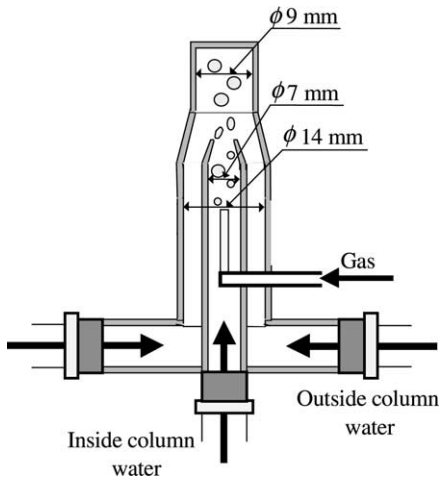

Fig. 2. Schematic diagram of mixing chamber.

overlapping and the bubbles deviated from the ellipsoidal bubble shape could be neglected. The axial gas velocity could also be calculated from a time for rising by a certain distance. More than

3000 bubbles were sampled to maintain similar statistics between the different combinations of gas and liquid flow rates. To evaluate the accuracy of the stereo image-processing method, flow parameters measured by the stereo image-processing method were cross-calibrated by other instrumentations such as a double-sensor conductivity probe and a rotameter. The statistical error of the double-sensor probe method for the interfacial area concentration measurements was estimated to be within $\pm 7\%$ for a sample size of ~ 1000 by means of a Monte Carlo method (Wu and Ishii, 1999). It was anticipated that a slight deformation might affect the interfacial area concentration. The analytical calculation showed that the interfacial area would not be changed so much (Hibiki et al., 1997). For example, when a spherical bubble was deformed to be a ellipsoidal bubble with the ratio of a major axis to a minor axis to be 2, the resulting increase in the interfacial area concentration was estimated to be less than 10% (Hibiki et al., 1997). Thus, a slight deviation of a bubble shape from an ellipsoidal bubble shape might not affect the measurement significantly. The calibration experiment was performed by using a flow loop with a 25.4-mm diameter tube installed at the Thermal-hydraulics and Reactor Safety Laboratory in Purdue University, since the double-sensor probe method might not be applicable to flow measurement in a small diameter tube due to the finite size of the probe. An excellent agreement was obtained between the interfacial area concentrations measured by the stereo image-processing method and the double sensor probe method within $\pm 6.95\%$. An example of the cross-calibration result is shown in Fig. 3. On the other hand, an excellent agreement was also obtained between the superficial gas velocities measured by the stereo image-processing method and the double sensor probe method within $\pm 13.3\%$. Thus, the measurement accuracy of the stereo image-processing method would be in the order of $\pm 10\%$. The stereo image-processing methodology was detailed in our previous paper (Takamasa and Watarai, 1996; Takamasa and Tomiyama, 1999). Due to the limitation of the test loop, the flow conditions were rather limited such that $\langle j_G \rangle = 0.013$ m/s and $\langle j_L \rangle = 0.58$ m/s, $\langle j_G \rangle = 0.052$ m/s and $\langle j_L \rangle = 0.58$ m/s, and $\langle j_G \rangle = 0.052$ m/s and $\langle j_L \rangle = 1.0$ m/s. Instead, the detailed measurements of axial flow developments were performed at six axial

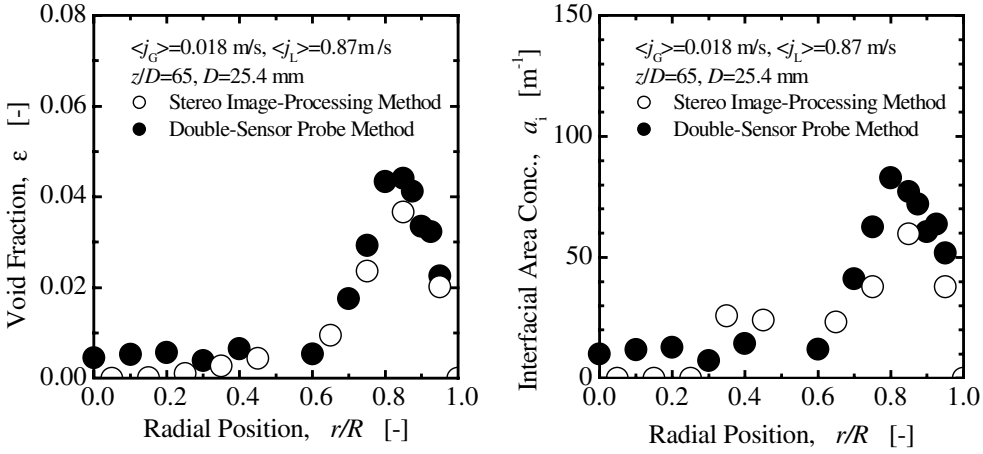

Fig. 3. Cross-calibration between stereo image-processing method and double-sensor probe method.

locations of $z/D = 3$, 6, 12, 24, 57, and 91. Thus, three data sets or 18 ($= 3 \times 6$) local flow data were acquired in the present experiment.

4. Result and discussion

4.1. Visual observation of interfacial area transport mechanism

Fig. 4 shows an example of temporally consecutive images taken at a fixed axial location of $z/D = 91$ for $\langle j_G \rangle = 0.052$ m/s and $\langle j_L \rangle = 0.58$ m/s. The left images are taken at an angle of 90° to respective right images. It is observed from this figure that a trailing bubble seems to catch up a preceding bubble, resulting in the bubble coalescence. It is known well that when bubbles enter the wake region of a preceding bubble, they will accelerate and may collide with the preceding one (Otake et al., 1977). According to Otake et al. (1977), there was a critical distance at which the preceding bubble began to exert noticeable influence on the trailing one. In their experiment, the critical distance was found to be about threefold to fourfold diameter of the preceding bubble. The relatively high bubble size-to-tube diameter ratio in a small diameter tube ($D_b/D \approx 0.33$ in this experimental condition) increases the probability of a trailing bubble to be within a projected area of a preceding bubble. On the other hand, since the radial motion of bubbles is restricted by the presence of the tube wall, bubble coalescence due to bubble random collision observed in medium tubes (25.4–50.8 mm) (Hibiki and Ishii, 1999; Hibiki et al., 2001) is unlikely to occur in a relatively small diameter tube. Thus, a major mechanism of bubble coalescence in a relatively small diameter tube may be acceleration of a trailing bubble by a wake effect of a preceding bubble. It should be noted here that bubble breakup is not marked in the present experiment ($\langle j_L \rangle \leqslant 1$ m/s) due to weak liquid turbulence.

4.2. Radial distribution of flow parameters

Fig. 5 shows axial developments of void fraction profiles. In the present experiment, various void fraction profiles are observed, depending on superficial gas and liquid velocities and axial

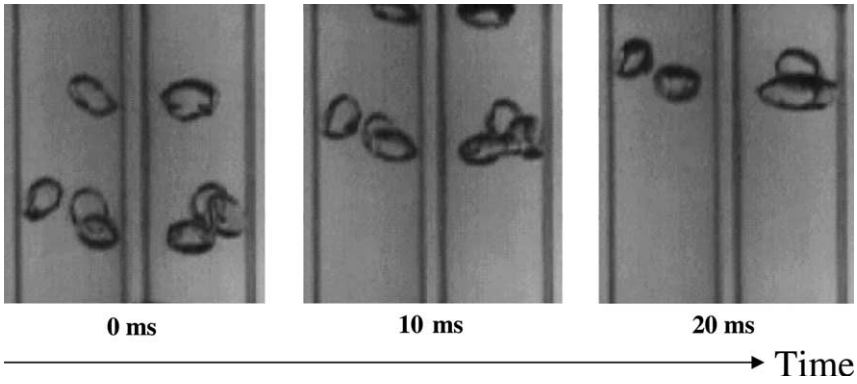

Fig. 4. Temporally consecutive images of bubble coalescence process taken at $z/D = 91$ for $\langle j_G \rangle = 0.052$ m/s and $\langle j_L \rangle = 0.58$ m/s.

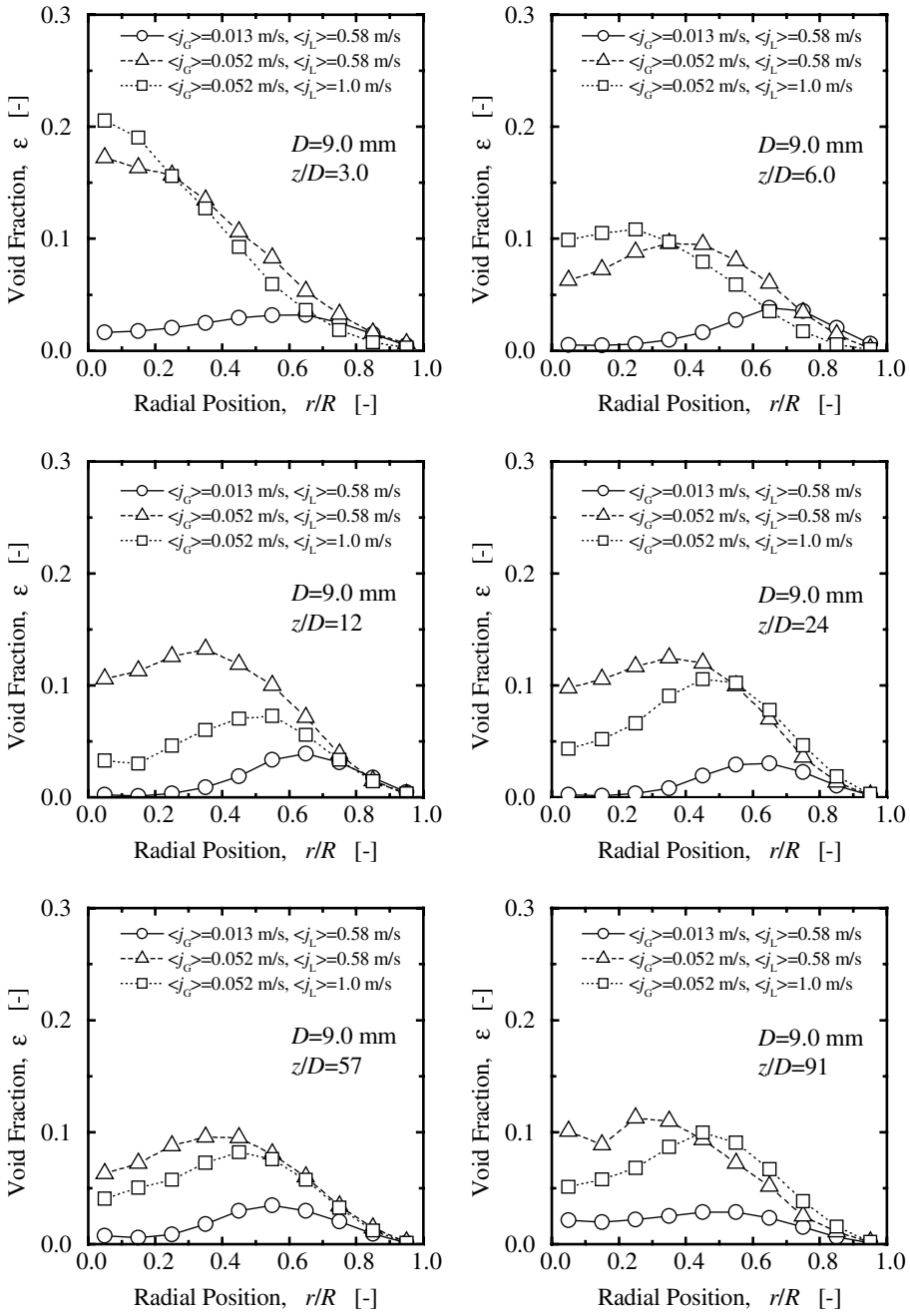

Fig. 5. Axial development of local void fraction profile.

location. Serizawa and Kataoka (1988) classified the phase distribution pattern of a vertical bubbly flow into four basic types of the distributions, that is, "wall peak", "intermediate peak",

"core peak", and "transition". The wall peak is characterized as sharp peak with relatively high void fraction near the channel wall and plateau with very low void fraction around the channel center. The intermediate peak is explained as broad peak in void fraction near the channel wall and plateau with medium void fraction around the channel center. The core peak is defined as broad peak around the channel center and no peak near the channel wall. The transition is described as a broad peak around the channel wall and center. It is known well that the initial void fraction profile is affected by the bubble injector design (Serizawa and Kataoka, 1988). The current bubble injector design generates an intermediate-peaked void distribution for $\langle j_G \rangle = 0.013$ m/s, $\langle j_L \rangle = 0.58$ m/s and $\langle \varepsilon \rangle = 2.09\%$ (◯) at the measuring station closest to the test section of $z/D = 3.0$. The increase in the superficial gas velocity augments the void fraction and tends to gather bubbles around the center of the channel, resulting in a core-peaked void distribution for $\langle j_G \rangle = 0.052$ m/s, $\langle j_L \rangle = 0.58$ m/s and $\langle \varepsilon \rangle = 5.82\%$ (△) at $z/D = 3.0$. Then, the increase in the superficial liquid velocity does not change the void fraction and its distribution significantly, resulting in a core-peaked void distribution for $\langle j_G \rangle = 0.052$ m/s, $\langle j_L \rangle = 1.0$ m/s and $\langle \varepsilon \rangle = 4.86\%$ (□) at $z/D = 3.0$ similar to that for $\langle j_G \rangle = 0.052$ m/s, $\langle j_L \rangle = 0.58$ m/s and $\langle \varepsilon \rangle = 5.82\%$ (△) at $z/D = 3.0$.

As a flow develops, bubbles tend to migrate towards the channel wall, since lift force acting on relatively small bubbles pushes the bubbles toward the channel wall. It was reported that in the flow conditions where wall peaking phenomena were observed in the void fraction profiles the peaks were approximately located at a distance equal to the bubble radius (Grossetete, 1995; Hibiki and Ishii, 1999). For example, the peak location for 3-mm diameter bubble in a 9.0- or 25.4-mm diameter tube is estimated to be about $r/R = 0.67$ and 0.88, respectively. Thus, even though wall-peaking phenomenon in a relatively small diameter tube is observed, the void peak is expected not to be located near the channel wall ($r/R \geqslant 0.67$).

For $\langle j_G \rangle = 0.013$ m/s and $\langle j_L \rangle = 0.58$ m/s, the wall peaking in the void fraction distribution is enhanced along the flow direction. For $\langle j_G \rangle = 0.052$ m/s, $\langle j_L \rangle = 0.58$ m/s and $\langle j_G \rangle = 0.052$ m/s, $\langle j_L \rangle = 1.0$ m/s, the wall peaking phenomena are not pronounced in comparison with that for $\langle j_G \rangle = 0.013$ m/s, $\langle j_L \rangle = 0.58$ m/s. Bubbles clustered around the channel center at $z/D = 3.0$ are redistributed to the channel, resulting in an intermediate-peaked void distribution. However, some bubbles seem to migrate toward the channel center at the downstream of $z/D = 57$, resulting in the increase of the void fraction around the channel center. Fig. 6 shows axial developments of bubble Sauter mean diameter profiles, corresponding to those of void fraction profiles in Fig. 5. As shown in this figure, the bubble size is increased along the flow direction due to the bubble coalescence and bubble expansion, resulting in the change of the bubble-migration direction. For $\langle j_G \rangle = 0.013$ m/s and $\langle j_L \rangle = 0.58$ m/s, the bubble Sauter mean diameter profiles are almost uniform along the channel radius at the upstream of $z/D = 57$, whereas relatively large bubbles formed by gradual bubble coalescence seem to migrate toward the channel center, resulting in a slight core-peaked distribution. For $\langle j_G \rangle = 0.052$ m/s and $\langle j_L \rangle = 0.58$ m/s, and $\langle j_G \rangle = 0.052$ m/s and $\langle j_L \rangle = 1.0$ m/s, the increases in void fraction may enhance the bubble coalescence, resulting in large bubbles. For the flow conditions, the bubble Sauter mean diameter profiles are almost uniform around the channel center with some decrease in size near the wall ($r/R \geqslant 0.6$).

Sekoguchi et al. (1974) observed the behaviors of isolated bubbles, which were introduced into vertical water flow in a 25 mm × 50 mm rectangular channel through a single nozzle. Based on their observations, they found that the bubble behaviors in dilute suspension flow might depend

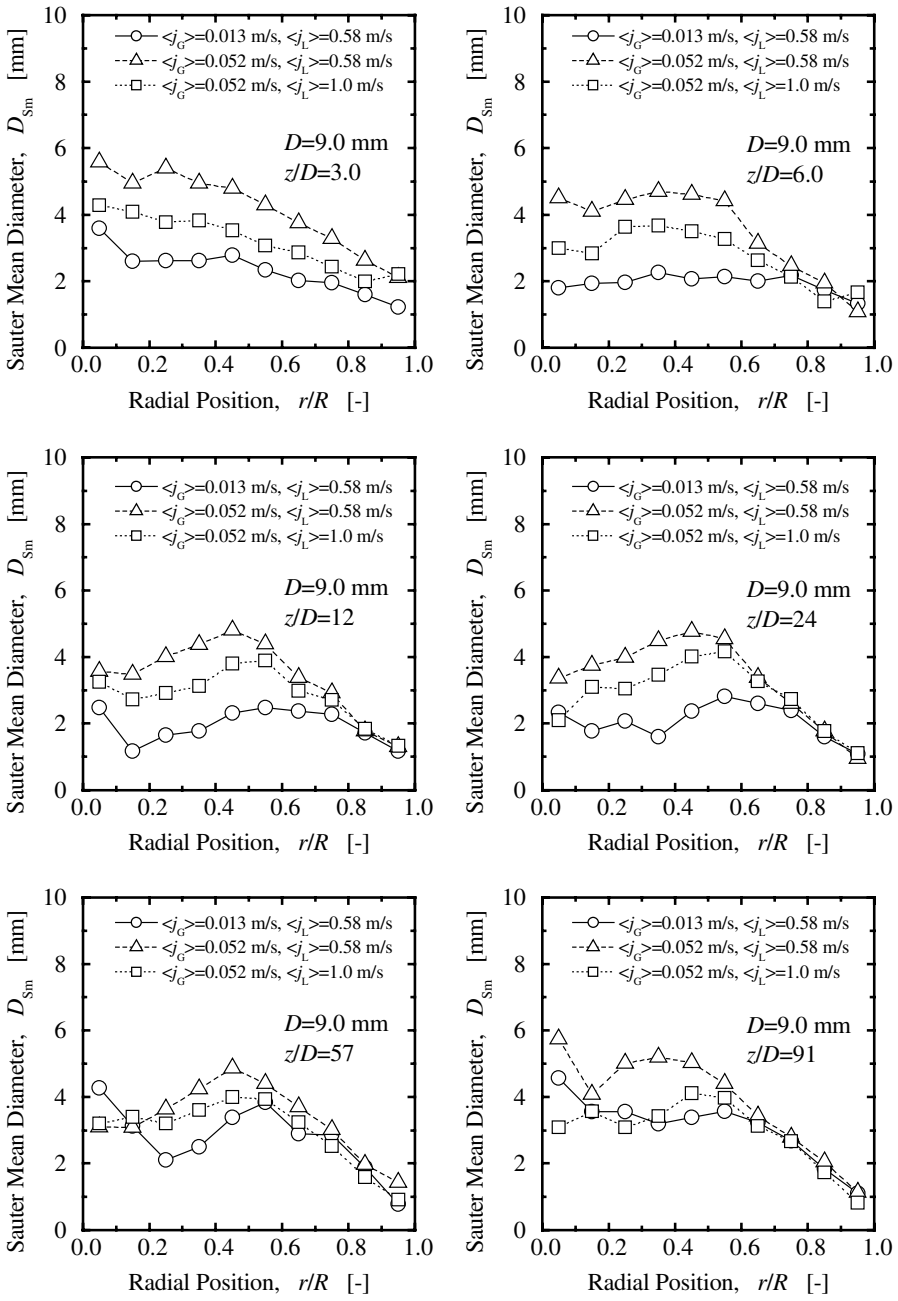

Fig. 6. Axial development of local bubble Sauter mean diameter profile.

on the bubble size and the bubble shape. In their experiment, only distorted ellipsoidal bubbles with a diameter smaller than nearly 5 mm tended to migrate toward the wall, whereas distorted ellipsoidal bubbles with a diameter larger than 5 mm and spherical bubbles rose in the channel

center. On the other hand, for the water velocity lower than 0.3 m/s, no bubbles were observed in the wall region. Zun (1988) also obtained a similar result. He performed an experiment to study void fraction radial profiles in upward vertical bubbly flow at very low average void fractions, around 0.5%. In his experiment, the wall void peaking flow regime existed both in laminar and turbulent bulk liquid flow. The experimental results on turbulent bulk liquid flow at Reynolds number near 1000 showed distinctive higher bubble concentration at the wall region if the bubble equivalent sphere diameter appeared in the range of 0.8–3.6 mm. Intermediate void profiles were observed at bubble sizes either between 0.6 and 0.8 mm or 3.6 and 5.1 mm. Bubbles smaller than 0.6 mm or larger than 5.1 mm tended to migrate towards at the channel center. Thus, the bubble migration characteristics to determine the void fraction profile are strongly dependent on the bubble size, which is determined by the interfacial area transport mechanism such as bubble coalescence, breakup and expansion or shrinkage.

Fig. 7 shows axial developments of interfacial area concentration profiles, corresponding to those of void fraction profiles in Fig. 5. The interfacial area concentration is directly proportional to the void fraction, if the bubble Sauter mean diameter is constant. Thus, the interfacial area concentration profiles for $\langle j_G \rangle = 0.013$ m/s and $\langle j_L \rangle = 0.58$ m/s are similar to the void fraction profiles, since the bubble Sauter mean diameter profiles are almost uniform along the channel radius. For $\langle j_G \rangle = 0.052$ m/s and $\langle j_L \rangle = 0.58$ m/s, and $\langle j_G \rangle = 0.052$ m/s and $\langle j_L \rangle = 1.0$ m/s, the interfacial area concentration profiles come to be almost uniform along the flow direction due to complicated bubble migration characteristics and bubble interactions.

Fig. 8 shows axial developments of gas velocity profiles, corresponding to those of void fraction profiles in Fig. 5. Due to very strong bubble coalescence and breakup at $z/D = 3.0$ and 6.0, the gas velocities at $z/D = 3.0$ and 6.0 can not be measured by the stereo image-processing method. The gas velocity profiles are almost uniform along the channel radius. It is well-known that for low liquid velocities ($\langle j_L \rangle \leqslant 1$ m/s) the introduction of bubbles into the liquid flow flattens the liquid velocity profile with a relatively steep decrease close to the wall (Serizawa and Kataoka, 1988; Hibiki and Ishii, 1999). The liquid velocity profile approaches to that of developed single-phase flow with the increase of void fraction. The effect of the bubble on the liquid velocity profile is diminishing with increasing gas and liquid velocities. For high liquid velocities ($\langle j_L \rangle > 1$ m/s), the liquid velocity profile comes to be the power-law profile as the flow develops. In the present experimental conditions, the bubble-induced turbulence would play an important role in determining the liquid velocity profile. The liquid velocity profiles in the present experiment are expected to be much flatter than that of developed single-phase flow. Since the gas velocity profile has the same tendency of the respective liquid velocity profile, almost flat distributions in the gas velocity profiles are observed in the experiment.

4.3. Axial development of one-dimensional flow parameters

In order to develop one-dimensional interfacial area transport equation, data on axial developments of area-averaged void fraction, interfacial area concentration and gas velocity are indispensable. Fig. 9 shows axial developments of the area-averaged flow parameters such as void fraction, interfacial area concentration, gas velocity, bubble Sauter mean diameter and bubble number density and the system pressure. The pressure changes along the flow direction in the present experiment are found to be within $\pm 3\%$, which indicates a negligible bubble expansion

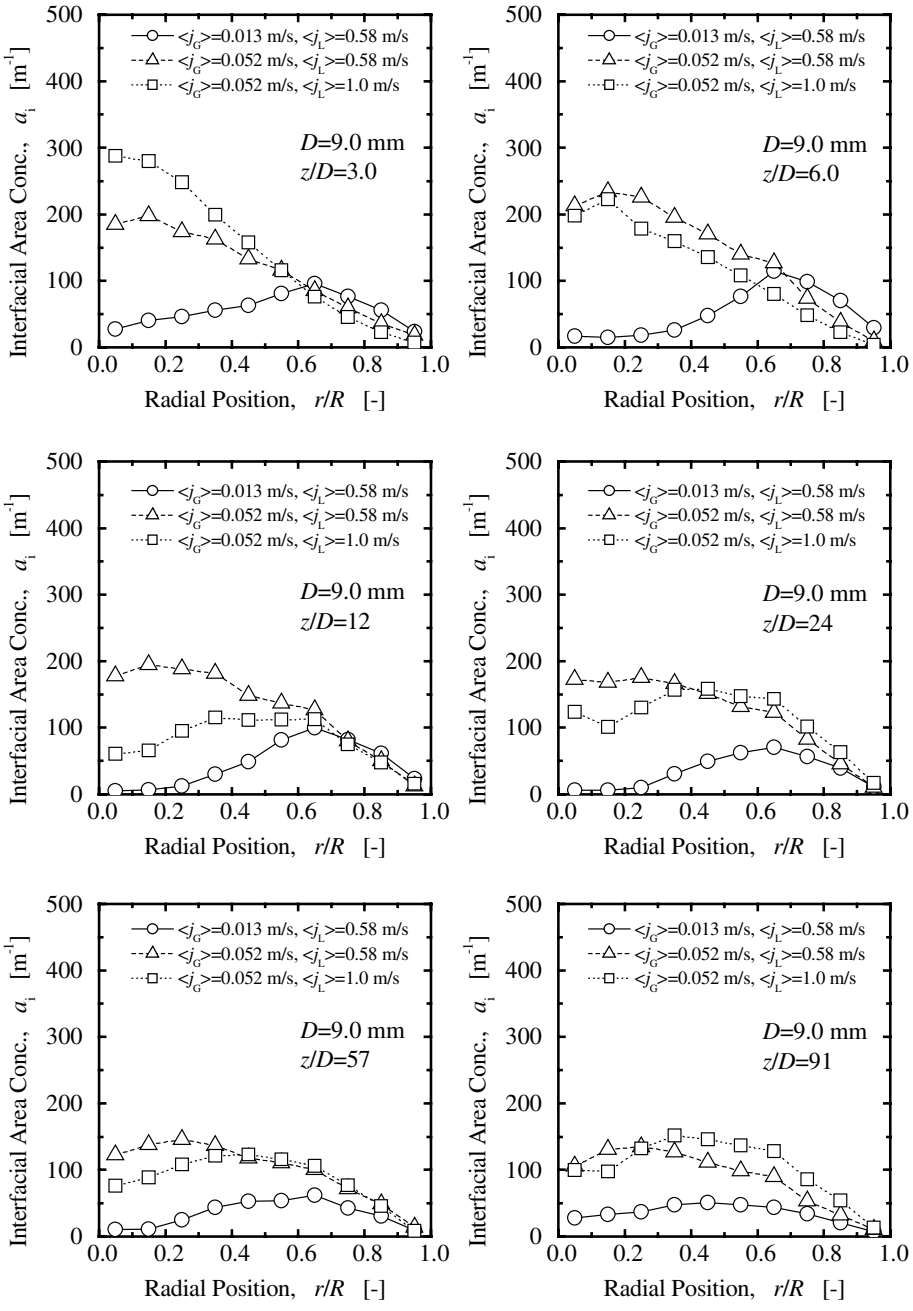

Fig. 7. Axial development of local interfacial area concentration profile.

along the flow direction. The area-averaged void fractions are almost constant along the flow direction with a slight decrease near the test section ($z/D \leqslant 24$). In this region ($z/D \leqslant 24$), bubbles are accelerating toward the rising velocity at the steady state. Thus, the void fractions in this

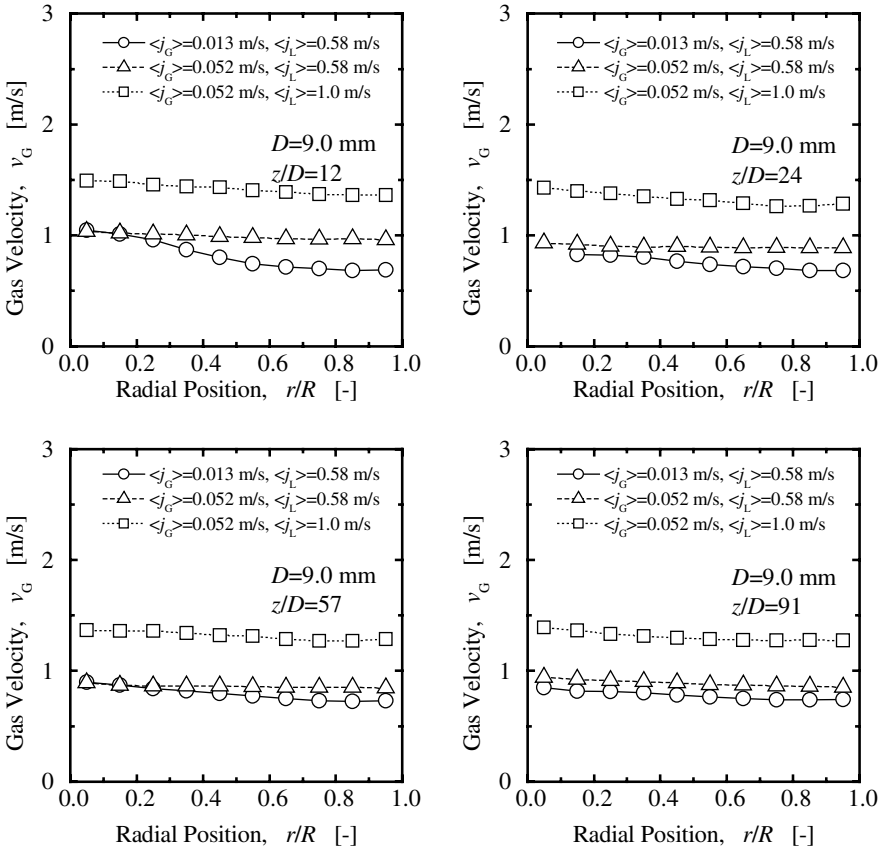

Fig. 8. Axial development of local gas velocity profile.

region ($z/D \leqslant 24$) are slightly higher than those in the region far from the test section inlet ($z/D > 24$). In the region ($z/D > 24$), the area-averaged gas velocities are almost constant along the flow direction. The area-averaged Sauter mean diameter measured for $\langle j_G \rangle = 0.013$ m/s and $\langle j_L \rangle = 0.58$ m/s is gradually increased along the flow direction due to bubble coalescence. On the other hand, the area-averaged bubble Sauter mean diameters for $\langle j_G \rangle = 0.052$ m/s and $\langle j_L \rangle = 0.58$ m/s, and $\langle j_G \rangle = 0.052$ m/s and $\langle j_L \rangle = 1.0$ m/s are almost uniform along the flow direction with a relatively steep decrease near the test section inlet. In this flow condition, the inlet bubble size created by the bubble generator may be too large, and the bubble breakup occurs at the test section inlet. The void fractions for $\langle j_G \rangle = 0.052$ m/s and $\langle j_L \rangle = 0.58$ m/s, and $\langle j_G \rangle = 0.052$ m/s and $\langle j_L \rangle = 1.0$ m/s are twice or three times higher than the void fraction for $\langle j_G \rangle = 0.013$ m/s and $\langle j_L \rangle = 0.58$ m/s. Since the bubble coalescence process for high void fraction is more enhanced than that for low void fraction. Thus, the bubble Sauter mean diameter for high void fraction may reach quasi steady-state condition at the closer location from the test section inlet. These bubble coalescence and breakup processes are clearly observed in the axial development of the bubble number density. As expected for bubbly flow, the axial changes of the area-averaged interfacial area concentration show a similar behavior of the axial change of the area-averaged void fraction.

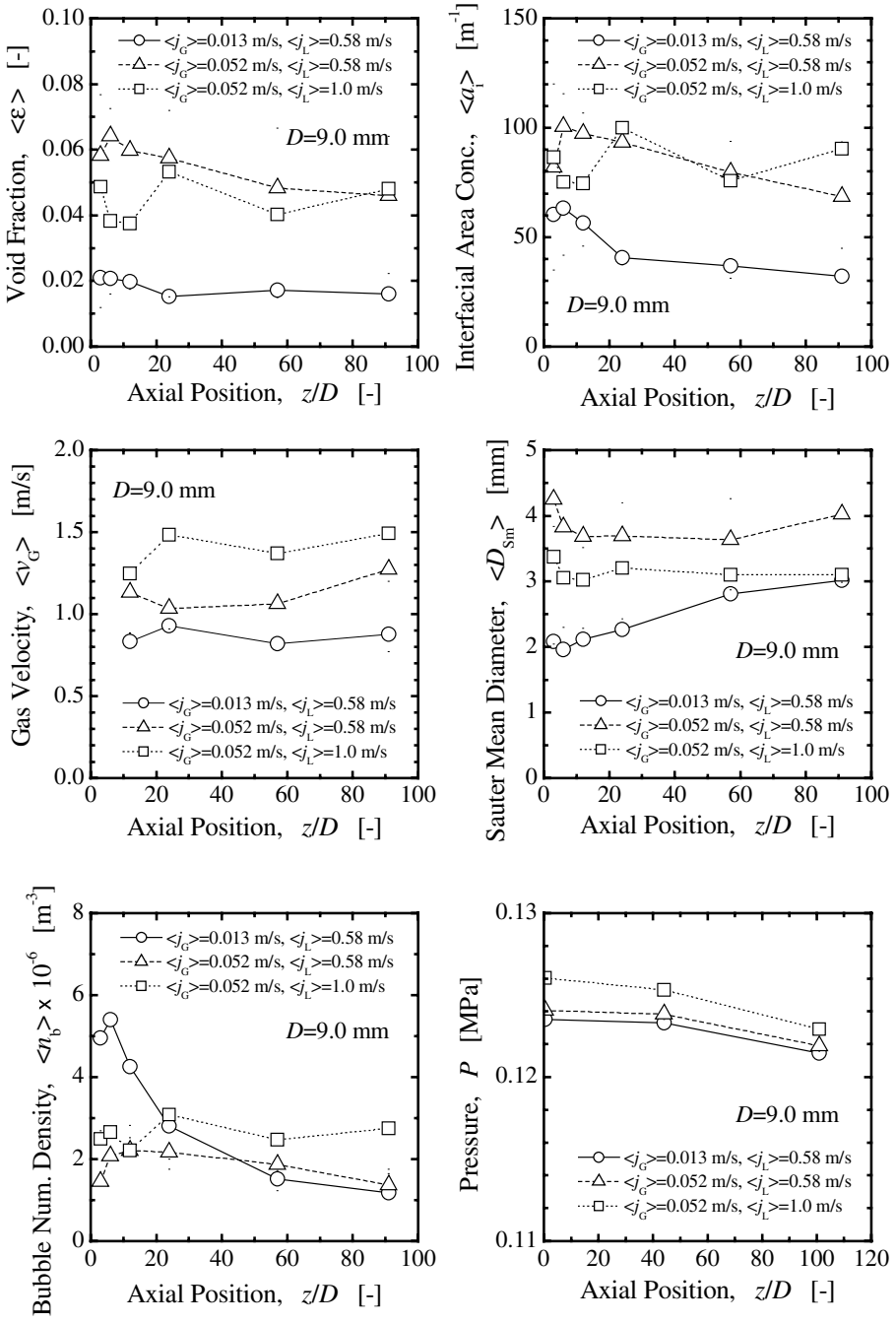

Fig. 9. Axial developments of area-averaged flow parameters and system pressure.

However, the area-averaged interfacial area concentration for $\langle j_G \rangle = 0.013$ m/s and $\langle j_L \rangle = 0.58$ m/s is decreased along the flow direction, since the bubble coalescence along the flow direction

decreases the bubble Sauter mean diameter. The interfacial area transport equation for medium tubes has been finalized by using data sets mainly taken at the downstream of $z/D = 6$ (Hibiki and Ishii, 2000a,b). To examine the applicability of the interfacial area transport equation to the flow very near the test section, detailed measurements of axial flow developments very near the test section are indispensable.

5. Conclusions

In relation to the development of the interfacial area transport equation, this study was conducted to correct accurate data sets on axial developments of local flow parameters such as void fraction, interfacial area concentration, and gas velocity. The local flow parameters of air–water bubbly flow in a vertical 9-mm-diameter tube were measured by means of a stereo image-processing method. The detailed flow measurements were performed at 6 axial locations of $z/D = 3$, 6, 12, 24, 57, and 91 for three flow conditions such as $\langle j_G \rangle = 0.013$ m/s and $\langle j_L \rangle = 0.58$ m/s, $\langle j_G \rangle = 0.052$ m/s and $\langle j_L \rangle = 0.58$ m/s, and $\langle j_G \rangle = 0.052$ m/s and $\langle j_L \rangle = 1.0$ m/s. The detailed discussions on the interfacial area transport were made based on the obtained data. The data would be expected to be used for the development of reliable constitutive relations which reflect the true transfer mechanisms in two-phase flow.

Acknowledgements

Part of this work was supported by Grant-in-Aid for Scientific Research from the Ministry of Education, Science, Sport and Culture (No.: 14580542).

References

Ebert, E. (Ed.), 1997. Proceedings of OECD/CSNI Workshop on Transient Thermal-hydraulic and Neutronic Codes Requirements, NUREG/CP-0159.

Grossetete, C., 1995. Experimental investigation and preliminary numerical simulations of void profile development. In: Proceedings of 2nd International Conference on Multiphase Flow, pp. IF1-1–IF1-10.

Hibiki, T., Ishii, M., 1999. Experimental study on interfacial area transport in bubbly two-phase flows. Int. Jr Heat Mass Trans. 42, 3019–3035.

Hibiki, T., Ishii, M., 2000a. One-group interfacial area transport of bubbly flows in vertical round tubes. Int. Jr Heat Mass Trans. 43, 2711–2726.

Hibiki, T., Ishii, M., 2000b. Two-group interfacial area transport equations at bubbly-to-slug flow transition. Nucl. Eng. Des. 202, 39–76.

Hibiki, T., Ishii, M., 2002. Development of one-group interfacial area transport equation in bubbly flow systems. Int. Jr Heat Mass Trans. 45, 2351–2372.

Hibiki, T., Ishii, M., Xiao, Z., 2001. Axial interfacial area transport of vertical bubbly flows. Int. Jr Heat Mass Trans. 44, 1869–1888.

Hibiki, T., Leung, W.H., Ishii, M., 1997. Measurement method of local interfacial area in two-phase flow using a double sensor probe. Purdue University Technical Report, PU/NE-97-5.

Kocamustafaogullari, G., Ishii, M., 1995. Foundation of the interfacial area transport equation and its closure relations. Int. Jr Heat Mass Trans. 38, 481–493.

Otake, T., Tone, S., Nakao, K., Mitsuhashi, Y., 1977. Coalescence and breakup of bubbles in liquids. Chem. Eng. Sci. 32, 377–383.

Sekoguchi, K., Sato, T., Honda, T., 1974. Two-phase bubbly flow (first report). Transactions of JSME 40, 1395–1403 (in Japanese).

Serizawa, A., Kataoka, I., 1988. Phase distribution in two-phase flow. In: Transient Phenomena in Multiphase Flow. Hemisphere, Washington, DC, pp. 175–225.

Takamasa, T., Tomiyama, A., 1999. Three-dimensional gas–liquid two-phase bubbly flow in a C-shaped tube. In: Proceedings of the 1999 NURETH-9 Conference.

Takamasa, T., Watarai, M., 1996. Measurements of bubble interfacial configurations in vertical bubbly flow using stereo image-processing method (SIM). In: Proceedings of ASME Fluid Engineering Division Summer Meeting, FED-239, vol. 4, pp. 175–190.

Wu, Q., Ishii, M., 1999. Sensitivity study on double-sensor conductivity probe for the measurement of interfacial area concentration. Int. J. Multiphase Flow 25, 155–173.

Wu, Q., Ishii, M., Uhle, J., 1998. Frame work of two-group model for interfacial area transport in vertical two-phase flows. Transactions of ANS 79, 351–352.

Zun, I., 1988. Transition from wall void peaking to core void peaking in turbulent bubbly flow. In: Transient Phenomena in Multiphase Flow. Hemisphere, Washington, DC, pp. 225–245.